RSC Advances

ROYAL SOCIETY OF CHEMISTRY

www.rsc.org/advances

Journal Name

COMMUNICATION

Enhanced Hydrogenation of Ethyl-levulinate to γ-valerolactone over $Ni^{\delta}O_x$ Stabilized Cu^+ surface sites

åReceived 00th January 20xx,
Accepted 00th January 20xx

DOI: 10.1039/x0xx00000x

www.rsc.org/

Junhua Zhu,[a,b] Yi Tang,[*,a] and Kangjian Tang,[*,b]

$CuNi^{\delta}O_x/SiO_2$ nanocatalysts with Cu-Ni activities below 5 nm were synthesized. The catalysts showed high performance for catalytic hydrogenation of ethyl-levulinate to γ-valerolactone at mild reaction conditions. The composition and structure of these nanocatalysts were characterized. It is shown that $Ni^{\delta}O_x$ play a key role in stabilizing Cu^+ against inactivation. To meet the requirement of industrial application, the $CuNi^{\delta}O_x/SiO_2$ nanocatalysts were tested under continuous reaction for over 2000 hours. The conversion and product selectivity maintained at 100% and above 95%, respectively.

Gamma-valerolactone (GVL) is an important chemical.[1-3] It can be used for producing liquid fuels,[4] intermediate for synthesizing fine chemicals,[5] solvent,[6-8] and flavoring agent.[9] GVL can be obtained from cellulose or hemi-cellulose by chemical methods, which make it worthy of a "green" material.[10] The chemical processes require a certain catalytic steps *via* formation of levulinic acid (LA) or its esters.[11] The homogeneous or heterogeneous catalysts for the conversion of LA or its esters to GVL have been studied.[12-21] Homogeneous catalysts included metal Ph, Ru, Ir complexes and heterogeneous catalysts included Ru, Pd, Au, Ag, Ni, Cu or their alloy on inertia C, Al_2O_3, SiO_2 or ZrO_2 supports.[16-21] In a batch reaction, the homogeneous catalyst of shvo-type ruthenium complex could easily give a 99.9% conversion.[12] Meanwhile, heterogeneous Ru/C, Ni/MoO_3, Cu/ZrO_2 catalysts could reach 99.9% conversion as well at the temperature of 190 °C, 140 °C, and 200 °C, respectively. However, to achieve sustainable GVL manufacture in industry,[22] the catalysts should: 1) be noble-metal-free;[23] 2) possess high activity, selectivity, and long-timed stability;[24] 3) use under mild conditions and friendly media; 4) work under continuous flow.[25] To the best of our knowledge, the reported catalysts could not meet all of these requirements. Homogeneous catalysts were expensive, and unable to use in continuous flow. Current heterogeneous noble-metal-free catalysts were suffered from their poor stability.[26]

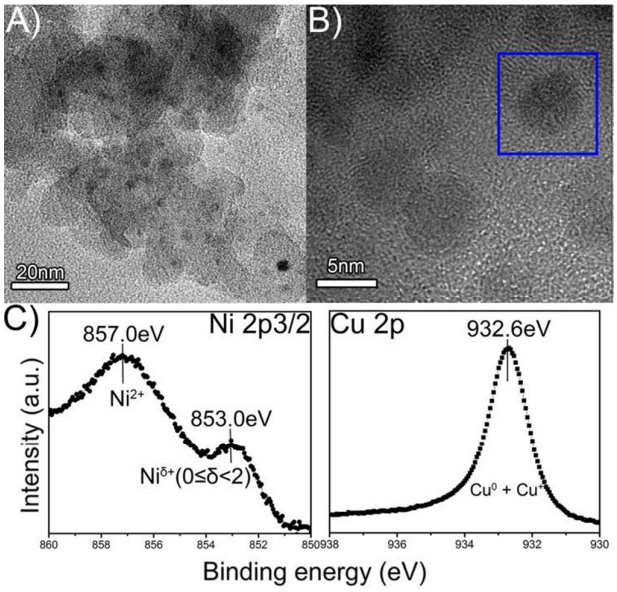

Figure 1. Structural characterizations and catalytic performance of the $CuNi^{\delta}O_x$ nanoparticles (NP). (a) HRTEM image on a 20nm domain. (b) HRTEM image of an individual $CuNi^{\delta}O_x$ NP. There were two or more suits of lattices shown by FFT result in blue box (see figure S1). (c) XPS core-level spectra of Ni2p3/2 and Cu2p, respectively.

Cu-based catalyst has been studied as a good candidate, the conversion could reach over 99.9%.[19] However, the activity of Cu-based catalyst is extremely low below 200 °C. Moreover, Cu-based catalyst easily deactivates over 230 °C because of the coke and aggregation of nanoactivities.[26] To meet the industrial requirements, it is important to improve the activity by stabilizing Cu^+ over 200°C or decrease the reaction temperature. So far, the efficient Cu-based catalyst is still hard to be developed. As known, the fabrication of multicomponent active sites, such as metal-metal oxide surface sites,[27] to facilitate the activation of reagents has been considered as an effective method for heterogeneous catalysts with improved

[a] Department of Chemistry, Fudan University, Shanghai 200433, (P.R. China) Fax: +86-21-65641740; Tel: +86-21-55664125 yitang@fudan.edu.cn
[b] Shanghai Research Institute of Petrochemical Technology, SINOPEC, Shanghai, 201208 (P. R. China). Fax: +86-21-68462283; Tel: +86-21-68462197-1202; E-mail: tangkj.sshy@sinopec.com
[c] Footnotes relating to the title and/or authors should appear here.
Electronic Supplementary Information (ESI) available: [details of any supplementary information available should be included here]. See DOI: 10.1039/x0xx00000x

performance. For example, Pt/FeO_x surface sites exhibit excellent performance in CO oxidation,[28] Au/CeO_x surface sites improve the activity of the water-gas shift reaction[29] *etc.* In a previous work, it have been studied the direct epoxidation of propylene over stabilized Cu^+ surface sites on titanium-modified Cu_2O.[30] The catalysis on O-terminal molecule on Cu-based catalysts was enhanced by Cu^+. Here, we reported a facile method to fabricate copper-nickel surface sites and disperse highly on the SiO_2 with grain size <5 nm in diameter. The Cu^+-$Ni^{\delta}O_x$ surface sites greatly improved the catalytic performance on hydrogenation of LA or ethyl-levulinate (EL) to γ-valerolactone under mild-condition. With this kind of catalyst, the catalysis could maintain high activity (over 99% conversion and 95% selectivity) for over 2000 hours without decay, and well meet the requirements of industry.

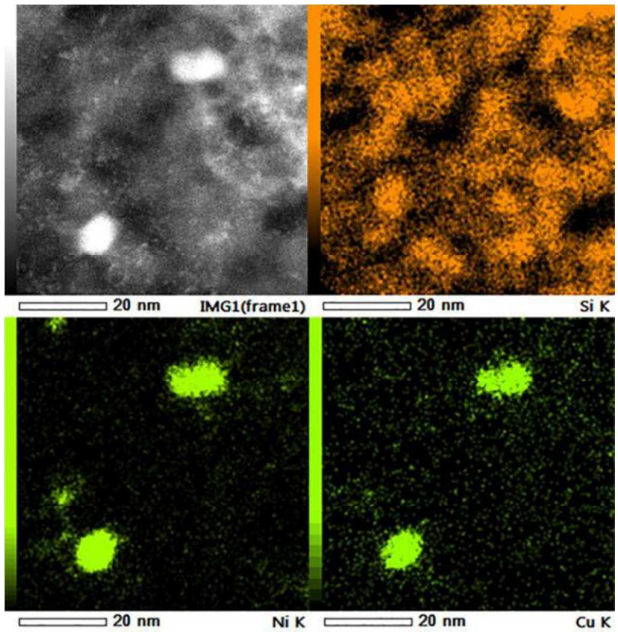

Figure 2. STEM-EDS elemental mapping on a 20nm domain of $CuNi^{\delta}O_x/SiO_2$ catalyst.

High resolution transmission electron microscopy (HRTEM) images (Figure 1a and b) reveal the activities on substrates are very fine nanoparticles with less than 5nm diameter. Lattice fringes with inter planar distances of 0.21nm, corresponding to Cu (111) planes, can be obviously observed (Figure S2). Energy dispersive spectroscopy (EDS) analysis shows that this domain mainly contains Cu, Ni and Si (Figure S3). Figure 1c shows the Cu x-ray photoelectron spectroscopy (XPS), suggesting the coexistence of Cu^+ oxidation state and Cu^0 metal state. The Ni XPS suggests the coexistence of Ni^{2+} oxidation state and Ni^{δ} ($0\leq\delta<2$) hemi-oxidation state. The $CuNi^{\delta}O_x/SiO_2$ catalyst was also characterized by an aberration-corrected scanning transmission electron microscopy (STEM). STEM-EDS measurements show that the copper and nickel are mixed well on the surface. EDX mapping analysis (Figure 2) on a 20nm domain and a larger area (Figure S4) reveals that the appearance of Cu is always coupled with the presence of Ni, which implies that the nickel atoms have strong bonding to copper atoms. Furthermore, series of XPS spectra on copper and nickel with different composition (Table S1, Table S2, Figure S5 and Figure S6) show that the amount of Cu^+ increases first and then decreases with increasing the amount of introduced nickel. From Figure S6 and Table S1, the amount of Cu^+ reaches maximum as 4% nickel is added. Figure 3 shows the X-ray diffraction (XRD) patterns of the as-prepared samples of $Ni(2\%)/SiO_2$, $Ni(8\%)/SiO_2$, $Cu(35\%)/SiO_2$, $Cu(35\%)Ni(4\%)/SiO_2$ and $Cu(35\%)Ni(8\%)/SiO_2$. Without Cu species, the XRD only show a broad peak of SiO_2 at around 25° when the amount of nickel below 2%. The characteristic peaks of NiO (111), (200) and (220) at 2θ of 37.3°, 43.4° and 62.8° can be observed when the nickel amount is 8%. Without Ni species, the XRD show characteristic peaks of Cu_2O (111) at 2θ of 37.1°, and peaks of Cu (111) and (200) at 2θ of 43.2° and 50.4°. Since the peaks at around 37° are affiliated to both Cu_2O and NiO and the peaks at around 43° are affiliated to Cu or NiO, we have to identify the structures of Ni and Cu species based on the peaks at 50.4° and 62.8°, respectively. From the XRD results of $Cu(35\%)Ni(4\%)/SiO_2$ and $Cu(35\%)Ni(8\%)/SiO_2$ samples, the peaks affiliating to metal Cu is very obvious but the peaks corresponding to copper oxides and nickel oxides are not so clear. Therefore, the Cu_2O, NiO and $Ni^{\delta}O_x$ with ultrafine grain size are highly dispersed. It can be concluded that without the introduction of the nickel, the Cu^+ is mainly offered by chrysocolla ($Cu_{2-x}Si_2O_5(OH)_x$ because the featured XRD peaks at 2θ of 30°~32° in the sample of $CuNi(0)/SiO_2$ can be observed. The Cu^+ is unstable during the reaction and easy to aggregate to be bigger grains due to the weak interaction between copper and silica. With the introduction of small amount of nickel, the chrysocolla cannot be formed. Ni-O species insert into Cu and Si and take the place of promoting Cu^+. With further increasing the nickel content, an optimized dispersion of copper species could be obtained based on the threshold of dispersing Ni-O species on silica. However, excess introduction of nickel leads to the aggregation of part of nickel oxide, on which the tiny copper sites have the chance of over growth.

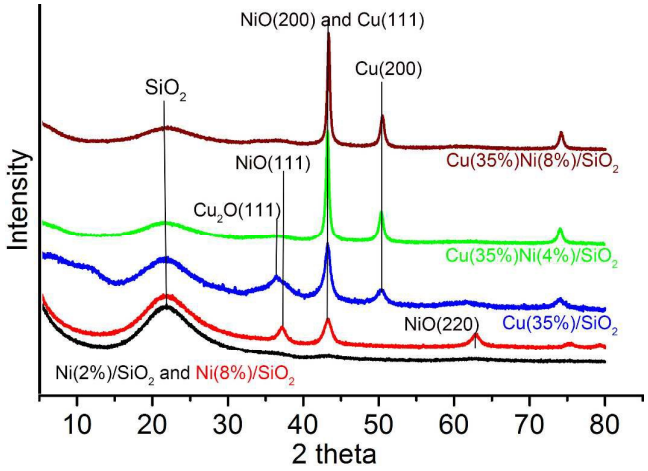

Figure 3. XRD curves of as-prepared catalysts.

Since the maximal Cu^+ are obtained, we tested the aimed reaction of catalytic hydrogenation of LA to GVL to evaluate the Cu^+-$Ni^{\delta}O_x$ surface sites effect. Figure 4a displays hydrogenation activity of Cu/SiO_2 and $CuNi^{\delta}O_x/SiO_2$ at the temperature of 230°C. Both catalysts could achieve over 99% LA conversion at this temperature. However, pure Cu/SiO_2 catalysts starts to lose its activity after 100 hours, and declines rapidly to below 50%. The reason for the degradation was investigated by TEM, as shown in Figure 4b. It is found that the Cu nanoparticles grow large obviously after this period of reaction, which leads to the activity decrease. In contrast, the $CuNi^{\delta}O_x/SiO_2$ can hold both its reaction

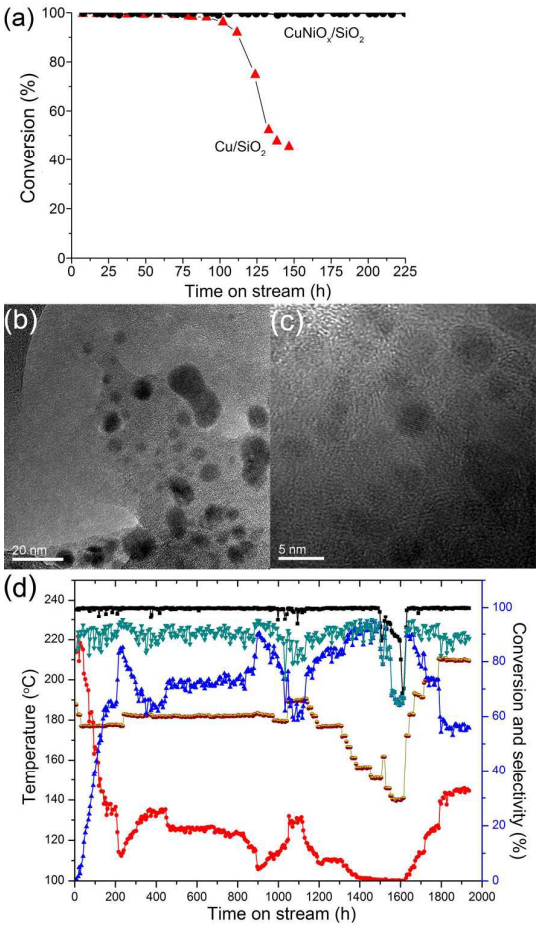

Figure 4. (a) LA conversions as a function of reaction time over $CuNi^{\delta}O_x/SiO_2$ and Cu/SiO_2 catalysts. (b) HRTEM image on a 20nm domain to verify the Cu/SiO_2 catalyst after 100 hours' reaction. (c) HRTEM image on a small domain to verify the $CuNi^{\delta}O_x/SiO_2$ catalyst after 200 hours' reaction. (d) EL conversion as a function of reaction time over $CuNi^{\delta}O_x/SiO_2$ catalyst. brown line indicates the changing of temperature; black line indicates the conversion rate; green line indicates the whole selectivity of (GVL+MTHF); blue line and red line indicate the selectivity of GVL and MTHF, respectively.

-activity and stability within the testing time. Figure 4c shows the compared TEM image of $CuNi^{\delta}O_x/SiO_2$ nanocatalyst after 200 hours' catalytic test. The particles' size was most hold at about 5nm (the XRD shown in figure S7 revealed that the structure of $CuNi^{\delta}O_x/SiO_2$ nanocatalyst could be kept as good as fresh ones). In industry, this noble-metal-free Cu^{+}-$Ni^{\delta}O_x$ catalysts featured by high activity, selectivity and stability should be work in friendly media and under mild continuous flow condition. LA is a kind of acidic chemical. When using H_2O as solvent, the LA solution is harmful to metal reactors and the separation of redundant H_2O after hydrogenation increases energy cost. The hydrogenation of ethyl-levulinate (EL) to GVL could solve the problem very well. Herein, the ethyl alcohol was used as solvent and reactant to LA. The reaction could be controlled in very low acidic environment and ethyl alcohol could be directly recycled. As shown in scheme S1, a controlled hydrogenation of EL to GVL at step 3 leads to GVL. Meanwhile, the chemical, methyl tetrahydrofuran (MTHF), at step 5 is a component of P-series fuels that are recently classified as alternative fuels by the U.S. department of Energy. It is projected to be used as a transportation fuel extender and has been successfully road-tested in fuel blends. Due to the attainability of GVL and MTHF, the targeted production of GVL and MTHF from EL becomes the focus of both academic and industrial research efforts. Figure 4d shows the detailed catalytic results on the optimized $CuNi^{\delta}O_x/SiO_2$ catalyst. During the 2000 hours test, we investigated its conversion, temperature-dependent selectivity, stability and distribution of byproducts. Compared to Cu/SiO_2 catalyst works at 230°C, the $CuNi^{\delta}O_x/SiO_2$ catalyst exhibits over 99% conversion at about 155 °C. Below 155 °C, the conversion decreases sharply. Slowly increasing the reaction temperature to 230 °C, the conversion could be hold continuously at over 99% without any decay. The whole selectivity (GVL+MTHF) could be kept over 90% within the temperature range.

Table 1 shows the detailed data of temperature-dependent selectivity of GVL and MTHF. GVL and MTHF are complementary on selectivity. Lower temperature is beneficial for producing GVL. The main product distribution could be adjusted by simply changing temperature. It can be seen that the GVL and MTHF could be obtained at the range from 150°C to 250°C. Below 150°C the conversion could not reach 99% and over 250°C, 1-pentanol became one of the main products. The optimal temperature for producing GVL is from 155°C to 175°C. Significantly, it is more than 60°C lower than that of the normal Cu-based catalyst. This work greatly extends the applied limitation of Cu-based catalysts on low-temperature catalysis. Table 2 listed the catalytic selectivity of Cu-Ni(0)/SiO_2 to Cu-Ni(8%)/SiO_2 catalysts at 230 °C. The selectivity increases first and then decreases with increasing the amount of nickel. Cu-Ni(4%)/SiO_2 shows the best catalytic performance. Combining the XPS and XRD results on series of Cu-Ni catalysts, it can be deduced that the highly dispersed and stabilized Cu^{+} is the key for this hydrogenation reaction and proper amount of nickel is necessary.

Table 1. Hydrogenation of EL to GVL and MTHF on Cu(35%)Ni(4%)/SiO_2 catalyst. (%)

T (°C)	Conversion (%)	MTHF	2-pentanol (%)	1-pentanol (%)	GVL	#others
140	79.37	0	0	0	95.14	4.86
160	99.92	1.37	0	0	95.22	3.41
180	99.96	4.63	0	0.07	91.70	3.60
200	99.99	7.60	0.02	0.23	87.85	4.30
220	99.99	17.24	0.16	1.87	75.85	4.88
240	99.99	25.30	0.27	4.40	63.27	6.76
260	99.99	67.00	0.69	18.11	4.82	9.38

[&]1,4-Pentanediol; * Ethyl Valerate; [#]Unidentified

Table 2. Hydrogenation of EL to GVL and MTHF on Cu(35%)Ni(#)/SiO_2 catalysts. (%)

Catalyst	Conversion	GVL+MTHF	1-pentanol	2-pentanol	# others
Ni (0%)	98.95	92.24	1.24	2.95	3.57
Ni (2%)	98.90	91.16	6.24	0.14	2.46
Ni (4%)	99.99	93.22	2.45	0.05	4.28
Ni (6%)	99.54	90.01	3.79	0.13	6.07
Ni (8%)	99.63	85.88	6.71	0.28	7.13

[#]others included: 1,4-pentanediol, ethyl valerate and some unidentified; Reaction conditions: 230□, 3.0Mpa. The data were acquired after reaction for 100 hours.

Conclusions

In conclusion, a Cu-based model catalyst by adding nickel to improve performance has been explored for the reaction of LA to GVL and EL to GVL. The proper amount of nickel could be dominant for the optimized catalysis. The $CuNi^{\delta}O_x$ oxide can effectively stabilize surface Cu^{+} and is ideal for using in industry as its over 99% conversion, 95% selectivity and over 2000 hours

stability. The strategy for the synthesis of stable mixed oxides provides a simple method in catalyst preparation and selectivity control. Results from the current study demonstrate the high potential to synthesize mixed metal oxides catalysts for practical applications.

Acknowledgements

The authors thank the partially financial support from the SINOPEC, National Natural Science Foundation of China (NSFC 21373272 and 2013CB93410).

Notes and references

† Electronic Supplementary Information (ESI) available: FFT pattern and HRTEM of on one nanoparticle; EDS and EDS mapping on small and large areas; XPS and LMM XAES results. See DOI: 10.1039/b000000x/

Experimental

The Cu-based catalysts were prepared by a co-precipitation method in which 0.20M aqueous solution of $Cu(NO_3)_2.3H_2O$ and proper amount of silica sol were taken and precipitated using 0.2M aqueous sodium carbonate at ambient temperature. The precipitate was aged further for 8 h at 60 ^oC. Then the mixture was separated by filtration and washed with deionized water to remove the traces of sodium. The solid thus obtained was dried in static oven at 110 ^oC for 24 h and calcined at 400 ^oC for 4 h. The weight percentage of copper in the Cu/SiO_2 catalyst was 35%. Cu^+-$Ni^{\delta}O_x/SiO_2$ catalysts were prepared by the same method, and different amount of $Ni(NO_3)_2.3H_2O$ were introduced at ambient temperature.

X-ray powder diffraction **(XRD)** patterns on series of catalysts were recorded in the range of 5~80° on Bruker D8 diffractometer using Cu Kα radiation with a scanning step 0.002°, voltage 40kV, and current 100mA. High resolution Transmission Electron Microscopy **(TEM)** was recorded on a FEI TECNAI-20 instrument with accelerating voltage of 200 kV. TEM specimen was prepared by dispersing the powder in alcohol by ultrasonic treatment and dropping onto a holey carbon film supported on a copper grid, and then dried in air. Scanning transmission electron microscopy **(STEM)** was performed on a double-corrected Titan Cubed 60-300 and a cold field emission gun was operated at 200 kV. STEM images were recorded using a high-angle annular dark-field (HAADF) detector. Temperature dependant XPS studies were performed on a Kratos AXIS Ultra DLD spectrometer equipped with a high temperature gas reaction cell. Catalysts reduction was carried out in the reaction cell with increasing temperature and feeding hydrogen. All the spectrum well collected with monochromatic Al K_α The C 1s peak at 284.8 eV was set as reference for binding energy calibration. All the spectrum processing and peak fitting were performed with CasaXPS.

All the reactions were carried out in a continuous flow, fixed-bed reactor and 5g catalysts were packed in the reactor. Prior to the reaction, the catalyst was reduced at 400 ^oC in H_2 flow. Ethyl-levulinate and ethanol solvent (EL/ethanol volume ratio was 1/1) were fed into the reactor using an injection pump, and the WHSV flow rate of EL was 0.6 h^{-1}. The reaction temperature was adjusted between 140^{o}C and 250^{o}C. The reaction pressure was maintained at 3.0 MPa. The molar ratio of hydrogen to EL was set as 50 (mol/mol). The hydrogenation products were analyzed using gas chromatography (Agilent 7890) equipped with a flame ionization detector and a capillary column (DB-200). The main products and byproducts were identified by GC-MS method on Agilent 5975C inert XL EI/CI MSD.

References

1. I.T. Horváth, H. Mehdi, V. Fabos, L. Boda, L.T. Mika, Green Chem. 2008, **10**, 238−242.
2. Y. Gu, F. Jérôme, Chem. Soc. Rev. 2013, **42**, 9550−9570.
3. X. Tang, X. Zeng, Z. Li, L. Hu, Y. Sun, S. Liu, T. Lei, L. Lin, Renew. Sust. Energy Rev. 2014, **40**, 608−620.
4. M.G. Al-Shaal, A. Dzierbinski,R. Palkovits, Green Chem. 2014, **16**, 1358−1364.
5. D. Wang, S.H. Hakim, D.M. Alonso, J.A. Dumesic, Chem. Commun. 2013, **49**, 7040−7042.
6. L. Qi, Y. Mui, S. Lo, M. Lui, G.R. Akien, I.T. Horváth, ACS Catal. 2014, **4**, 1470−1477.
7. J.S. Luterbacher, J.M. Rand, M.D. Alonso, J. Han, J.T. Youngquist, C.T. Maravelias, B.F. Pfleger, J.A. Dumesic, Science, 2014, **343**, 277−280.
8. E.I. Gürbüz, J.M. Gallo, D.M. Alonso, S.G. Wettstein, W.Y. Lim, J.A. Dumesic, Angew. Chem. Int. Ed. 2013, **52**, 1270−1274.
9. S. Tanaka, K. Fukuda, T. Asada, (Kao Corp.). Patent No. EP1555261A1, 2005.
10. G. Centi, R.A. van Santen, Catalysis for Renewables, Eds. Wiley-VCH: Weinheim, 2007.
11. R.J. van Putten, J.C. van der Waal, E, de Jong, C. B, Rasrendra, H.J. Heeres,J.G. de Vries, Chem. Rev. 2013, **133**, 1499−1597.
12. Y. Blum, D. Reshef, Y. Shvo, Tetrahedron Lett. 1981, 22, 1541−1544.
13. J. Deng, Y. Wang, T. Pan, Q. Xu, Q. Guo, Y. Fu, ChemSusChem, 2013, **6,** 1163−1167.
14. C. Ortiz-Cervantes, J. García, J. Inorg. Chim. Acta. 2013, **397**, 124−128.
15. W. Li, J. Xie, H. Lin, Q. Zhou, Green Chem. 2012, **14**, 2388−2390.
16. M.G. Al-Shaal, W.R.H. Wright, R. Palkovits, Green Chem. 2012, 14, 1260−1263.
17. K. Yan, T. Lafleur, G. Wu, J. Liao, C. Ceng, X. Xie, Appl. Catal. A: Gen. 2013, **468**, 52−58.
18. X. Du, L. He, S. Zhao, Y. Liu, Y. Cao, H. He, K. Fan, Angew. Chem. Int. Ed. 2011, **50**, 7815−7819.
19. J. Yuan, S, Li, L. Yu, Y. Liu, Y. Cao, H. He, K. Fan, Energy Environ. Sci. 2013, **6**, 3308−3313.
20. A.M. Hengne, A.V. Malawadkar, N.S. Biradar, C.V. Rode, RSC Adv. 2014, **4,** 9730−9736.
21. Y. Yang, G. Gao, X. Zhang, F. Li, ACS Catal. 2014, 4, 1419−1425.
22. P.C. Bruijnincx, Y. Román-Leshko, Catal. Sci. Technol. 2014. **4,** 2180-2181
23. K. Yan, A. Chen, Fuel 2014, 115, 101−108.
24. D. Pletcher, F. Walsh, Industrial Electrochemistry, Springer: London, U.K., 1990, 83.
25. C. Wiles, P. Watts, Green Chem. 2014, **16**, 55−62.
26. B. Putrakumar, N. Nagaraju, V.P. Kumar, K.V.R. Chary, Catalysis Today, 2015, **250**, 209–217
27. Q. Fu, W. Li, X. Bao, et al., Science, 2010, 328, 1141–1144.M. S. Chen, D. W. Goodman, Science, 2004, **306**, 252–255.
28. B. Qiao, A. Wang, X. Yang, L.F. Allard, Z. Jiang, Y. Cui, J. Liu, J. Li, T. Zhang, Nat. Chem. 2011, **3**, 634–641.
29. J. A. Rodriguez, S. Ma, P. Liu, J. Hrbek, J. Evans, M. Pérez, Science, 2007, **318**, 1757–1760.
30. X. Yang, S. Kattel, K. Xiong, K. Mudiyanselage, S. Rykov, S.D. Senanayake, J.A. Rodriguez, P. Liu, D.J. Stacchiola, J.G. Chen, Angew. Chem. Int. Ed. 2015, **54,** 11946 –11951.

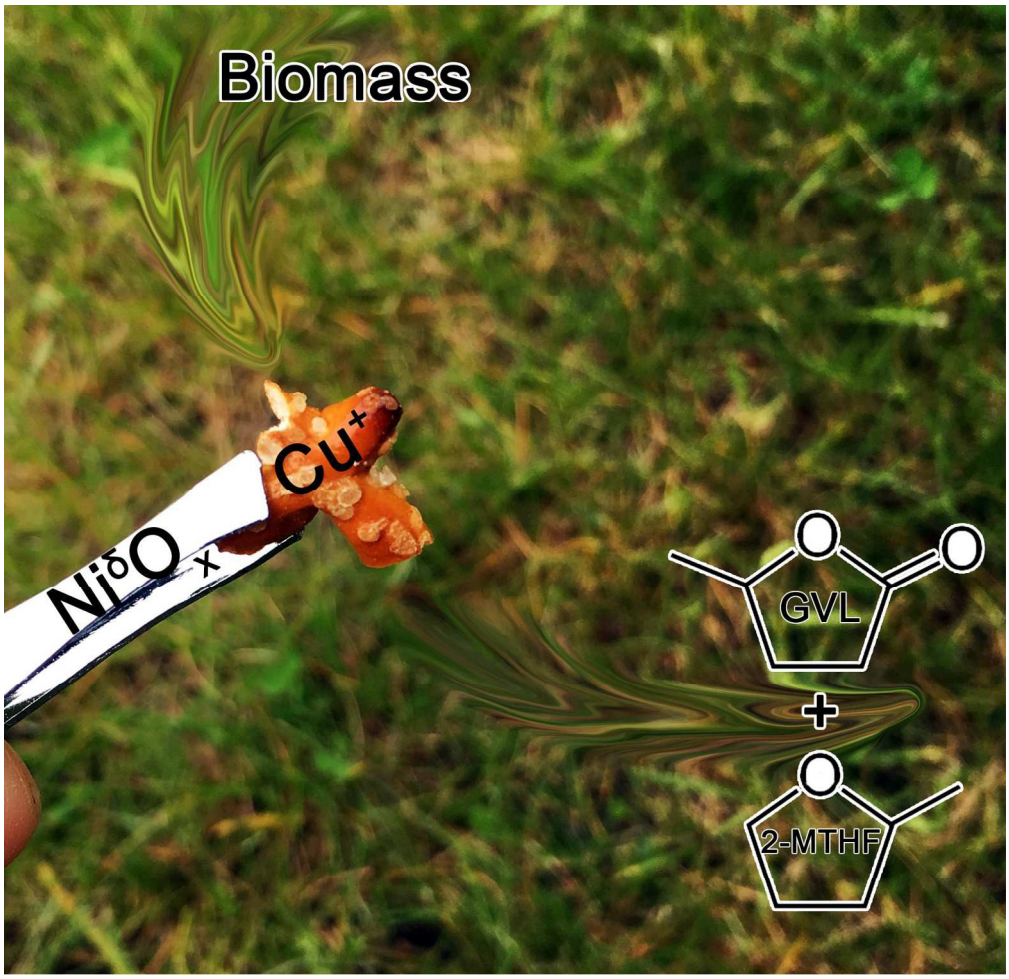

156x151mm (300 x 300 DPI)